Original Article

Evaluation of cold atmospheric pressure plasma irradiation of water as a method of singlet oxygen generation

Tokuko Takajo,[1] Hiroki Nagahama,[1] Katsuya Zuinen,[1] Kazunori Tsuchida,[1] Akitoshi Okino,[2] and Kazunori Anzai[1,*]

[1]Faculty of Pharmaceutical Sciences, Nihon Pharmaceutical University, 10281 Komuro, Ina-machi, Kitaadachi-gun, Saitama 362-0806, Japan
[2]Laboratory for Future Interdisciplinary Research of Science and Technology, Institute of Innovative Research, Tokyo Institute of Technology, 4259 Nagatsuta, Midori-ku, Yokohama 226-8502, Japan

(Received 6 October, 2022; Accepted 16 December, 2022; Released online in J-STAGE as advance publication 16 May, 2023)

We used cold atmospheric pressure plasma jet to examine in detail $^1O_2$ generation in water. ESR with 2,2,5,5-tetramethyl-3-pyrroline-3-carboxamide, a secondary amine probe, was used for the detection of $^1O_2$. Nitroxide radical formation was detected after cold atmospheric pressure plasma jet irradiation of a 2,2,5,5-tetramethyl-3-pyrroline-3-carboxamide solution. An $^1O_2$ scavenger/quencher inhibited the ESR signal intensity induced by cold atmospheric pressure plasma jet irradiation, but this inhibition was not 100%. As 2,2,5,5-tetramethyl-3-pyrroline-3-carboxamide reacts with oxidizing species other than $^1O_2$, it was assumed that the signal intensity inhibited by NaN_3 corresponds to only the nitroxide radical generated by $^1O_2$. The concentration of $^1O_2$ produced by cold atmospheric pressure plasma jet irradiation for 60 s was estimated at 8 μM. When this $^1O_2$ generation was compared to methods of $^1O_2$ generation like rose bengal photoirradiation and 4-methyl-1,4-etheno-2,3-benzodioxin-1(4*H*)-propanoic acid (endoperoxide) thermal decomposition, $^1O_2$ generation was found to be, in decreasing order, rose bengal photoirradiation ≥ cold atmospheric pressure plasma jet > endoperoxide thermal decomposition. Cold atmospheric pressure plasma jet is presumed to not specifically generate $^1O_2$, but can be used to mimic states of oxidative stress involving multiple ROS.

Key Words: **cold atmospheric pressure plasma jet, singlet oxygen, ESR, rose bengal, endoperoxide**

Plasma, the fourth state of matter, is a partially ionized gas consisting of electrons, photons, atoms, radicals, and various excited and non-excited molecules. Advances in plasma technology have enabled plasma generation at near atmospheric pressure and room temperature, referred to as cold atmospheric pressure plasma (CAP). CAP has potential in biomedical applications such as chronic wound treatment,[1–4] infection control,[5–8] and cancer therapy.[9–12] CAP induces, in the liquid phase and inside cells, reactive oxygen species (ROS) formation, such as hydroxyl radicals ($^{\bullet}OH$), superoxide anion radicals ($^{\bullet}O_2^-$), atomic oxygen and reactive nitrogen species (RNS), such as nitric oxide (NO), nitrogen dioxide (NO_2) and peroxynitrite($ONOO^-$).[13–16] Previously we reported the generation of reactive species such as $^{\bullet}OH$, $^{\bullet}H$, and H_2O_2 in water by cold atmospheric pressure plasma jet (CAPPJ) irradiation.[17]

Atmospheric molecular oxygen (triplet oxygen) is a stable form of molecular oxygen. Singlet oxygen ($^1O_2$) is, however, highly reactive and considered a ROS. In living organisms, $^1O_2$ is considered responsible for certain disorders, including photoaging, skin damage, and erythropoietic porphyria.[18–20] On the other hand, the cell death and tissue destruction induced by $^1O_2$ are used in photodynamic therapy,[21,22] which shows promise as a cancer therapeutic. Thus, $^1O_2$ itself and/or $^1O_2$ scavengers/quenchers may be used as treatments. From this perspective, it is important to establish easy and reliable methods for $^1O_2$ measurement and generation. Several measurement methods exist, including electron spin resonance (ESR) spectroscopy with sterically hindered secondary amine probes, near-infrared luminescence, spectrophotometric analysis with diphenylbenzofuran, and fluorescence measurement with specific fluorescent probes.[23–29] Along with measuring $^1O_2$, facile $^1O_2$ generation is also important. Widely used methods for $^1O_2$ generation include photoirradiation of photosensitizers such as rose bengal [30,31] and porphyrins, and by endoperoxide thermal decomposition.

CAPPJ irradiation of water generates various ROS [17,32–34] with the species type and amount generated controlled by irradiation parameters and reaction conditions.[35] For example, we reported the influence of irradiation distance on $^{\bullet}OH$ and H_2O_2 formation.[17] Reports also indicate $^1O_2$ generation by CAP irradiation.[15,35,36] In the present paper, we used CAPPJ with helium as a carrier gas to evaluate CAPPJ as a $^1O_2$ generating method in water. ESR with a secondary amine probe was used for $^1O_2$ detection and results were compared with other $^1O_2$ generation methods.

Materials and Methods

Chemicals. Ultrapure helium gas (>99.999%) was obtained from Saisan Co., Ltd. (Saitama, Japan). 2,2,6,6-tetramethyl-4-piperidone (TEMPD), 2,2,6,6-tetramethyl-4-piperidinol (TEMP-OH), 2,2,5,5-tetramethyl-3-pyrroline-3-carboxamide (TPC) and carbamoyl-PROXYL were obtained from Sigma-Aldrich Co. Ltd. (St. Louis, MO). Histidine (His), sodium azide (NaN_3) and 1,4-diazabicyclo[2,2,2] octane (DABCO) were obtained from Fujifilm Wako Pure Chemical Industries Ltd. (Osaka, Japan). 4-Methyl-1,4-etheno-2,3-benzodioxin-1(4*H*)-propanoic acid (endoperoxide, EP) was obtained from WAKEN B TECH Co. Ltd. (Kyoto, Japan). All reagents were of the highest grade available and used without further purification.

Irradiation of water with CAPPJ. CAPPJ was generated using a plasma head (TPN-20; NU global, Nagoya, Japan) and an electric regulating unit (PN-110TPG; NU global) with helium as the carrier gas. The helium gas flow rate was regulated by a mass flow controller (CUBE GM2; Fcon Co., Ltd, Nankoku, Kochi, Japan), and set at 5 L/min except for the experiment of Fig. 3, where the flow rate of 3 L/min was used. The flow rate of 3 L/min resulted in slightly greater nitroxide radical formation

*To whom correspondence should be addressed.
E-mail: anzai@nichiyaku.ac.jp

doi: 10.3164/jcbn.22-111

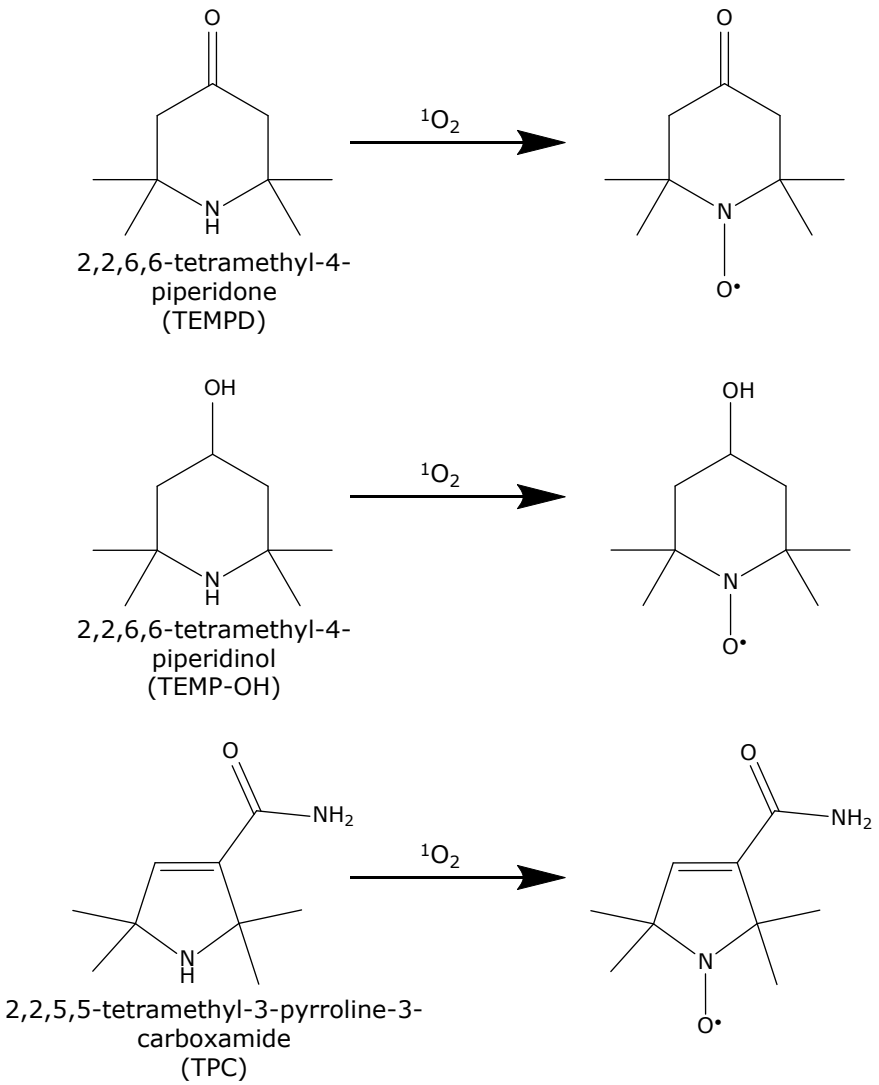

Fig. 1. Chemical structure and reaction of $^1O_2$ detection probes.

(approximately 20% increase) than the 5 L/min condition (unpublished result). The 1 ml sample solution was placed in a glass container, inner diameter 2 cm and 2 cm in height, and irradiated with CAPPJ at a distance of 1.5 cm between the solution surface and plasma jet tip.

ESR measurement. The CAPPJ irradiated solution was immediately transferred to a quartz flat cell, and ESR measured. The X-band ESR spectra were recorded using a JES-FA100 ESR spectrometer (JEOL Ltd., Akishima, Tokyo, Japan). Mn^{2+} was used as the external standard. The signal intensity was calculated by dividing the signal height at the lowest magnetic field side of the nitroxide radical by the signal height of Mn^{2+}. ESR spectra were analyzed with a WinRad ESR Data Analyzer (Radical Research Co., Ltd., Hino, Tokyo, Japan).

Generation of $^1O_2$ from EP or rose bengal solution photoirradiation. The $^1O_2$ generating reagent, EP, was heated at 40°C to generate $^1O_2$ by thermal decomposition. Alternatively, $^1O_2$ was generated by visible light irradiation of rose bengal solution using a Schott Megalight 100 with halogen lamp (Moritex Corporation, Yokohama, Japan) as the light source at a distance of 3 cm.

Results

Oxidation of $^1O_2$ detector probes by CAPPJ irradiation of water. The sterically hindered secondary amines such as TEMP-OH, TEMPD and TPC are often used as $^1O_2$ detector probes. TEMPD and TEMP-OH with a piperidine skeleton, and TPC with a pyrrolidine skeleton, react with $^1O_2$ to form stable nitroxide radicals (Fig. 1) which are subsequently detected by ESR.

By irradiating a TEMPD solution (0.2 mM) with CAPPJ for 1 min, a three-line ESR signal, typical for nitroxide radicals, was observed (Fig. 2A). When a TEMP-OH solution (0.2 mM) was irradiated with CAPPJ, signal splitting in the ESR spectrum was observed (Fig. 2B), which may be due to oxidation of the hydroxy group at the 4' position of the TEMP-OH piperidine skeleton by $^{\bullet}OH$.[28,37] When a TPC solution was irradiated by CAPPJ, a similar three-line signal was detected as in the TEMPD solution (Fig. 2C). No nitroxide radical was observed for all three secondary amine probes in the presence of helium gas flow without discharge of the CAPPJ. Although nitroxide radicals were formed and detected by all three detection probes, TPC was superior to TEMP-OH and TEMPD, as TEMP-OH shows ESR signal splitting and TEMPD is easily oxidized by air

doi: 10.3164/jcbn.22-111

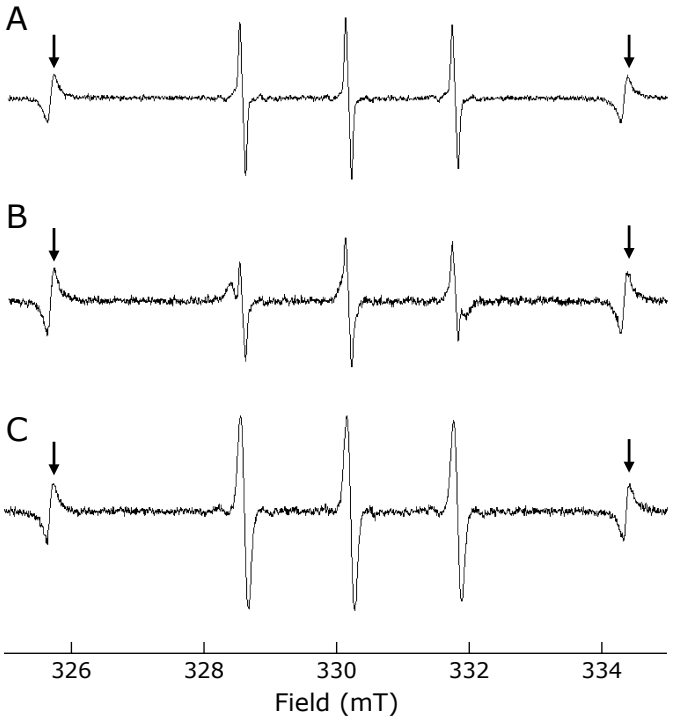

Fig. 2. ESR spectra obtained after CAPPJ irradiation of secondary amine solutions. Each solution was irradiated by CAPPJ for 1 min at distance of 1.5 cm. The helium gas flow rate was set to 5 L/min. (A) 0.2 mM TEMPD solution, (B) 0.2 mM TEMP-OH solution, and (C) 1 mM TPC solution. MnO_2 signal (arrows) is shown as the external standard.

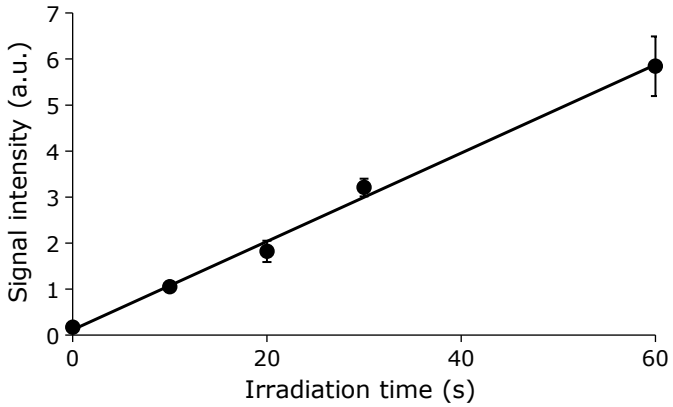

Fig. 3. Change in the ESR signal intensity of the nitroxide radical by CAPPJ irradiation time. TPC solution (2 mM, 1 ml) was irradiated with CAPPJ at a distance of 1.5 cm and irradiation time varied. The helium gas flow rate was 3 L/min. After irradiation, the solution was immediately transferred to a quartz flat cell, and ESR measured. Error bar shows SD (n = 3).

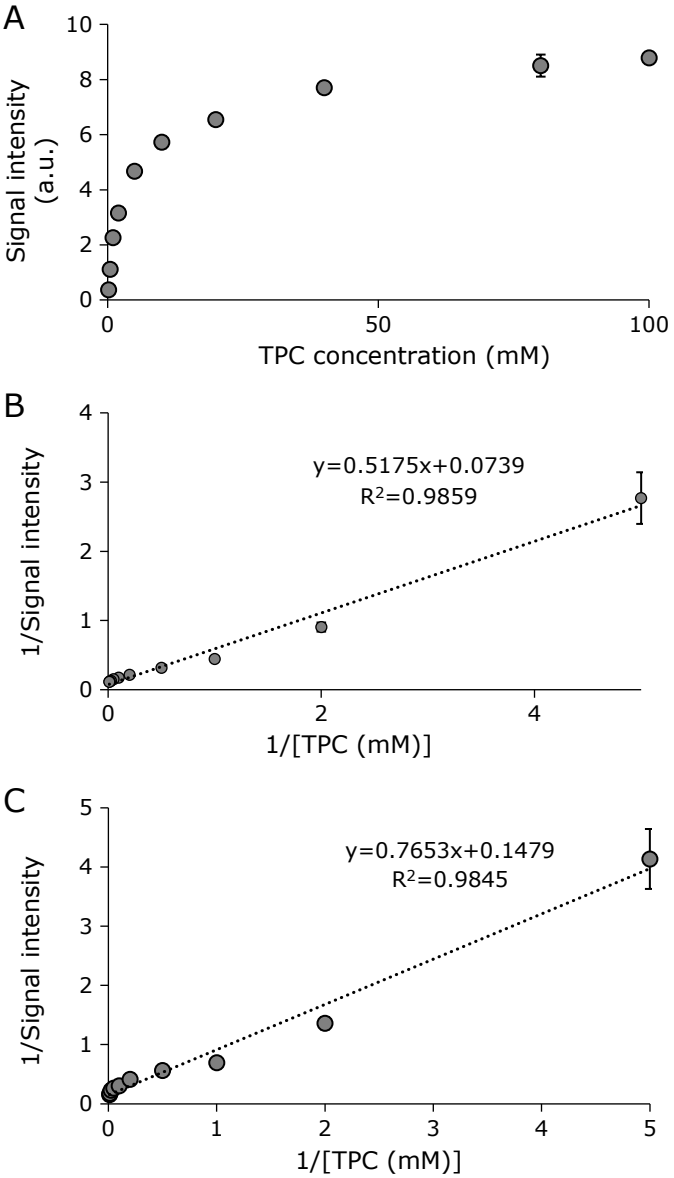

Fig. 4. Change in ESR signal intensity by TPC solution concentration. TPC solution (1 ml) with varying concentrations (0.2–100 mM) was irradiated by CAPPJ at a distance of 1.5 cm. The helium gas flow rate was set to 5 L/min. After the irradiation, the solution was immediately transferred to a quartz flat cell, and ESR spectra measured. Error bar shows SD (n = 3). (A) The signal intensity is plotted against the TPC concentration. The irradiation time was 60 s. (B) Double reciprocal plot of the data used for the graph (A). The reciprocal of the signal intensity is plotted against the reciprocal of the TPC concentration. (C) Double reciprocal plot of the data of 30 s irradiation. The reciprocal of the signal intensity is plotted against the reciprocal of the TPC concentration.

and dissolved oxygen.[28] We therefore used TPC in subsequent experiments.

Time-dependent oxidation of TPC by CAPPJ irradiation. The ESR signal intensity increased linearly during the 1 min CAPPJ irradiation of the TPC solution (2 mM, 1 ml) (Fig. 3). The same tendency was observed in the irradiation of TEMPD and TEMP-OH solutions (data not shown). Therefore, it is plausible that the secondary amine moiety of the $^1O_2$ detection probes was oxidized to form nitroxide radicals by $^1O_2$.

Effect of TPC concentration on ESR signal intensity. Varying concentrations of TPC solutions were irradiated with CAPPJ and ESR spectra were measured. When the TPC concentration increased, the ESR spectra intensity increased. This increase was not linear, however, and saturated at high TPC concentrations (Fig. 4A). A double reciprocal plot[38] (pseudo-Lineweaver-Burk plot with the reciprocal of signal intensity versus the reciprocal of TPC concentration) yielded a straight line (Fig. 4B and C). The value of the y-intercept was 0.0739 when the 60 s irradiation data was used. The inverse of this value

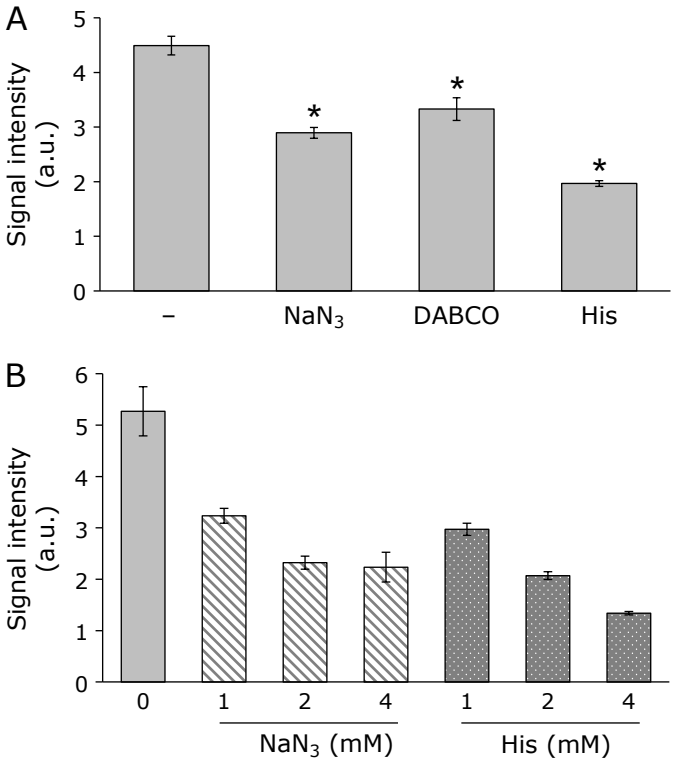

Fig. 5. Change in the ESR signal intensity by the addition of $^1O_2$ quencher/scavenger. (A) The mixture (1 ml) of TPC solution (2 mM) and $^1O_2$ scavenger (2 mM) was irradiated by CAPPJ for 60 s. The solution was irradiated at a distance of 1.5 cm. The helium gas flow rate was set to 5 L/min. Immediately after irradiation, the solution was transferred to a quartz flat cell and the ESR spectrum measured. Error bar shows SD ($n = 3$). *$p<0.01$ vs control by t test. (B) Effect of quencher/scavenger concentration on the signal intensity. The mixture (1 ml) of TPC solution (2 mM) and NaN_3 solution (1, 2, 4 mM) or His solution (1, 2, 4 mM) was irradiated with CAPPJ for 60 s. Error bar shows SD ($n = 3$).

(1/0.0739 = 13.5) corresponds to the quantity of nitroxide radicals produced over 60 s in the presence of a large excess of TPC. When the 30 s irradiation data was used, the y-intercept was 0.1479 and the inverse of this value was 1/0.1479 = 6.8. In other words, as there was sufficient TPC in the system, it is presumed that the TPC reacts with most of the $^1O_2$ generated. Nitroxide radical concentrations were then estimated by a calibration curve, generated by relating the signal intensity and radical concentration for carbamoyl-PROXYL solutions of known concentrations. The amount of nitroxide radical detected was estimated to be 17.5 μM for 60 s of CAPPJ irradiation and 8.7 μM when irradiated for 30 s.

Effect of $^1O_2$ quenchers/scavenger on nitroxide radical production. To verify nitroxide radical formation due to $^1O_2$, we added His as a $^1O_2$ scavenger, or NaN_3 and DABCO as a $^1O_2$ quencher (Fig. 5A). The ESR signal intensity was significantly suppressed by His, NaN_3, and DABCO addition. The suppression was 56 ± 1.4% by 2 mM His, 36 ± 0.8% by 2 mM NaN_3, and 26 ± 4.6% by 2 mM DABCO. Furthermore, NaN_3 and His inhibited signal intensity in a concentration dependent manner (Fig. 5B). The inhibition was 57 ± 4.5% in the presence of 4 mM NaN_3 and 74 ± 0.5% in the presence of 4 mM His. However, complete inhibition was not observed even in the presence of 4 mM quencher/scavenger.

Effect of mannitol on nitroxide radical production. To examine whether $^{\bullet}OH$ is involved in the nitroxide radical formation, we added mannitol, a scavenger of $^{\bullet}OH$, to the solution. As

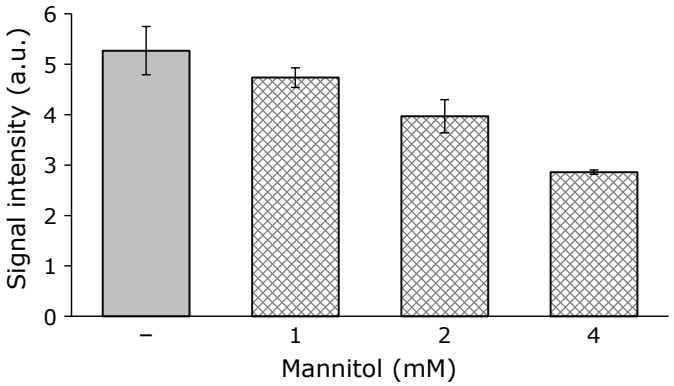

Fig. 6. Change in the ESR signal intensity by mannitol addition, a hydroxyl radical scavenger. The mixture (1 ml) of TPC solution (2 mM) and mannitol solution (1–4 mM) was irradiated with CAPPJ for 60 s. The solution was irradiated at 1.5 cm. The helium gas flow rate was set to 5 L/min. Immediately after irradiation, the solution was transferred to a quartz flat cell and the ESR was measured. Error bar shows SD ($n = 3$).

shown in Fig. 6, the nitroxide radical ESR signal intensity was inhibited 10%, 25%, and 46% by 1 mM, 2 mM, and 4 mM mannitol, respectively.

Comparison of nitroxide radical formation by CAPPJ to other $^1O_2$ generation methods. We compared CAPPJ $^1O_2$ generation to that by rose bengal photoirradiation and EP thermal decomposition (Fig. 7). The ESR signal intensity observed from CAPPJ irradiation was inhibited by addition of a large amount of NaN_3 (100 mM). The inhibition was 28 ± 2.8% at 30 s and 35 ± 3.0% at 60 s. The ESR signal intensity observed in rose bengal photoirradiation (0.2 mM) for 30 s and 60 s was similar as that observed for 30 and 60 s CAPPJ irradiation. Addition of a large amount of NaN_3 (100 mM) to the rose bengal system was accompanied by decreased signal intensity. The signal inhibition was 55 ± 5.7% at 30 s and 65 ± 5.2% at 60 s. For the thermal decomposition of EP, unlike the CAPPJ irradiation and the photoirradiation of rose bengal, the ESR signal could not be detected within a few minutes, despite a higher EP concentration (the SOAC assay used 0.4–0.8 mM, while we used 2 mM) and higher temperature (the SOAC assay used 35°C, while we used 40°C).[25,26,39] Increasing the reaction time to 60 min, enabled ESR signal detection, although the intensity was very low. The addition of 100 mM NaN_3 resulted in 77 ± 5.2% inhibition on the ESR signal intensity at 60 min.

Discussion

Of the several $^1O_2$ measurement methods, ESR with sterically hindered secondary amine probes is often used.[27,29,38] The secondary amine probe is oxidized to a stable nitroxide radical, which is detected by ESR. Of the several secondary amine probes,[29,38,40–42] we compared three, TEMPD, TEMP-OH, and TPC, and found that TPC was superior (Fig. 2) and therefore, TPC was chosen for the present work.

The ESR signal intensity increased linearly during the 1 min CAPPJ irradiation of the TPC solution, indicating $^1O_2$ formation. The concentration of the resultant nitroxide radical is related to the concentration of generated oxidant. We estimated the amount of $^1O_2$ generated by CAPPJ irradiation by assuming 100% $^1O_2$ reaction with TPC. By increasing the TPC concentration, the reaction between the oxidant and TPC increases. As shown in Fig. 4A, the ESR signal intensity saturated at higher TPC concentrations, and the double reciprocal plot yielded a straight line. The intercept of the plot y-axis shows the inverse of the

doi: 10.3164/jcbn.22-111

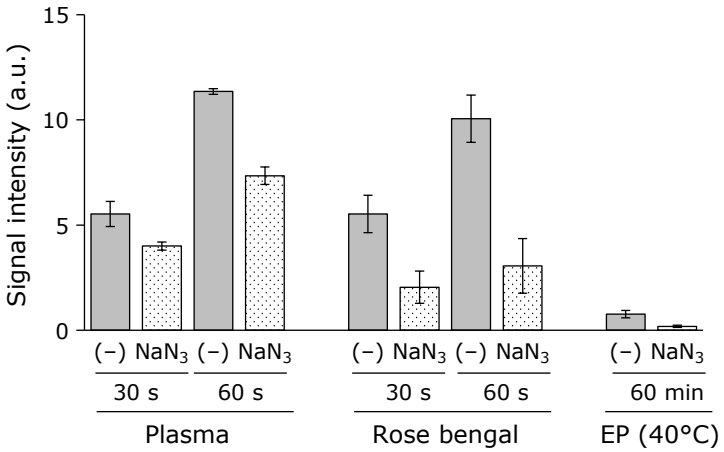

Fig. 7. Comparison of $^1O_2$ generation by CAPPJ with other $^1O_2$ generation methods in the presence and absence of NaN_3. TPC concentration was 75 mM and NaN_3 concentration was 100 mM. TPC solution was irradiated with CAPPJ at a distance of 1.5 cm for 30 or 60 s, with or without NaN_3. The helium gas flow rate was set to 5 L/min. The mixed solutions of TPC and rose bengal (0.2 mM) were irradiated with visible light from a distance of 3 cm for 30 or 60 s, with or without NaN_3. The mixed solutions of TPC and EP (3 mM) were incubated at 40°C for 60 min, with or without NaN_3. Immediately after irradiation, the solution was transferred to a quartz flat cell and the ESR was measured. Error bar shows SD (n = 3).

signal intensity at an infinite TPC concentration. This signal intensity was then converted to nitroxide radical concentration using the calibration curve. The nitroxide radical concentrations were thus estimated to be 17.5 μM and 8.7 μM for the 60 s and 30 s sample irradiations, respectively. However, these estimations are not equal to the $^1O_2$ concentration generated as the oxidation reaction efficiency by $^1O_2$ is not 100% and oxidation species other than $^1O_2$ contribute to the signal increase. Although the secondary amine probes we used are frequently used for $^1O_2$ detection, probe reaction with other ROS is also possible. Indeed, Jablonowski *et al.* described nitroxide radical formation by the reaction of secondary amine probes with O_3 and $^{\bullet}O$.[43]

We estimated the contribution of $^1O_2$ in nitroxide radical production among the total oxidizing species formed by CAPPJ irradiation. NaN_3, DABCO, and histidine, which scavenge/quench $^1O_2$, significantly inhibited the nitroxide radical signal intensity induced by CAPPJ irradiation (Fig. 5). This observation confirms the involvement of oxidizing species other than $^1O_2$ in nitroxide radical formation. The ESR signal intensity was also inhibited by the presence of mannitol (Fig. 6), implicating $^{\bullet}OH$ as an oxidizing species. Considering that nitroxide radical formation inhibition by NaN_3 and histidine was about 60–70% and mannitol inhibition was about 45%, $^{\bullet}OH$ is clearly another major oxidizing species produced during CAPPJ irradiation that contributes to nitroxide radical formation. Indeed, we previously reported $^{\bullet}OH$ generation by CAPPJ irradiation under the same conditions as the present study.[17] The concentration of $^{\bullet}OH$ generated by 60 s irradiation was high, approximately 270 μM (unpublished result).

As TPC also reacts with oxidizing species other than $^1O_2$, the signal intensity inhibited by NaN_3 can be regarded as the nitroxide radical generated by only $^1O_2$.[15] Here, we estimated the concentration of $^1O_2$ generated by CAPPJ irradiation in the presence of 75 mM TPC and 100 mM NaN_3, the same concentrations as previously used [15] and compare with results obtained by rose bengal photo-irradiation and EP thermal-decomposition. For EP thermal decomposition, the ESR signal was very small, suggesting limited $^1O_2$ generation. As the SOAC measurement is performed over a long time, the EP decomposition forming $^1O_2$ is slow. In the case of CAPPJ irradiation and rose bengal photoirradiation, nitroxide radical formation was greater than that from EP decomposition. The nitroxide radical formation amount was CAPPJ > rose bengal > EP. On the other hand, inhibition by NaN_3 was 35% for CAPPJ, 65% for rose bengal, and 77% for EP, which indicates EP thermal decomposition generates relatively pure $^1O_2$. Considering total amounts of the nitroxide formed and inhibition by NaN_3, the order of $^1O_2$ generation was estimated as rose bengal ≥ CAPPJ > EP. Since the rose bengal photoirradiation uses visible right, the energy of the light is quenched when a colored compound is used. Therefore, the rose begal photoirradiation is not applicable to the sample with colors. In contrast, the color of the sample does not affect the$^1O_2$ generation by CAPPJ irradiation.

It is reported that not only $^1O_2$ but also $^{\bullet}OH$ is generated in rose bengal photoirradiation.[28] Therefore, $^{\bullet}OH$ may be an active oxidizing species in the rose bengal photoirradiation. We reported $^{\bullet}OH$, $^{\bullet}H$, and H_2O_2 formation by CAPPJ irradiation.[17] Contribution of O_3 in nitroxide radical formation was also reported.[34,43] In our approach, the contribution of O_3 cannot be ruled out as we detected a slight ozone-like smell during CAPPJ irradiation, however the O_3 contribution is likely small given the large estimated $^{\bullet}OH$ contribution, at around 45% of total signal intensity.

Only 30–50% of the values obtained in Fig. 4B and C are generated by $^1O_2$. From this, the total nitroxide concentration, 17.5 μM estimated at an infinite TPC concentration, converts to around 5–8 μM of $^1O_2$ produced by 60 s CAPPJ irradiation. This value is the same order of magnitude as the amount of $^1O_2$ produced reported by Takamatsu *et al.*[15] We have values of about 270 μM for $^{\bullet}OH$ generation (unpublished data) and about 60 μM for H_2O_2 generation[17] by CAPPJ irradiation under the same conditions as the present study. The amount of these ROS produced were more than one order of magnitude larger than the amount of $^1O_2$ produced estimated in this study. To increase $^1O_2$ production by CAPPJ irradiation, various parameters can be tuned. Changing the carrier gas is one method to increase $^1O_2$ production. Indeed, carrier gas selection is reported to change the amount of $^1O_2$ generated.[15] When O_2 and CO_2 are used as carrier gases, $^1O_2$ generation was 63 μM and 90 μM, respectively.

In conclusion, $^1O_2$ generation by CAPPJ irradiation under these conditions was confirmed. CAPPJ irradiation, however, generates reactive species other than $^1O_2$ and the amount of $^1O_2$ generated is rather low at a few μM. Therefore, CAPPJ with helium as the carrier gas under our reaction conditions does not generate $^1O_2$ specifically. However, the system is easy to operate and superior to rose bengal photoirradiation for CAPPJ irradiation. The CAPPJ can be used as an oxidative stress inducing system with multiple kinds of ROS.

Author Contributions

TT contributed to the study design, data acquisition, and manuscript drafting. HN and KZ collected data. KT and AO contributed to critical revision of the manuscript. KA supervised the study, data interpretation and critical revision of the manuscript.

Acknowledgments

This work was supported in part by JSPS KAKENHI Grant Number 16K08203 to KA. A part of this research is based on the Cooperative Research Project of Research Center for Biomedical Engineering.

Conflict of Interest

We have not received any financial support or other benefits from commercial sources for the work reported in the manuscript. None of the authors have financial interests that could create a potential conflict of interest or the appearance of a conflict of interest with regard to this work.

References

1 Emmert S, Pantermehl S, Foth A, *et al*. Combining biocompatible and biodegradable scaffolds and cold atmospheric plasma for chronic wound regeneration. *Int J Mol Sci* 2021; **22**: 9199.

2 Shimatani A, Toyoda H, Orita K, *et al*. *In vivo* study on the healing of bone defect treated with non-thermal atmospheric pressure gas discharge plasma. *PLoS One* 2021; **16**: e0255861.

3 Haertel B, von Woedtke T, Weltmann KD, Lindequist U. Non-thermal atmospheric-pressure plasma possible application in wound healing. *Biomol Ther (Seoul)* 2014; **22**: 477–490.

4 Isbary G, Morfill G, Schmidt HU, *et al*. A first prospective randomized controlled trial to decrease bacterial load using cold atmospheric argon plasma on chronic wounds in patients. *Br J Dermatol* 2010; **163**: 78–82.

5 Yang Y, Wang H, Zhou H, *et al*. Protective effect of the golden staphyloxanthin biosynthesis pathway on *Staphylococcus aureus* under cold atmospheric plasma treatment. *Appl Environ Microbiol* 2020; **86**: e01998-19.

6 Lou BS, Lai CH, Chu TP, *et al*. Parameters affecting the antimicrobial properties of cold atmospheric plasma jet. *J Clin Med* 2019; **8**: 1930.

7 Mai-Prochnow A, Murphy AB, McLean KM, Kong MG, Ostrikov KK. Atmospheric pressure plasmas: infection control and bacterial responses. *Int J Antimicrob Agents* 2014; **43**: 508–517.

8 Isbary G, Shimizu T, Zimmermann JL, Thomas HM, Morfill GE, Stolz W. Cold atmospheric plasma for local infection control and subsequent pain reduction in a patient with chronic post-operative ear infection. *New Microbes New Infect* 2013; **1**: 41–43.

9 Nakamura K, Peng Y, Utsumi F, *et al*. Novel intraperitoneal treatment with non-thermal plasma-activated medium inhibits metastatic potential of ovarian cancer cells. *Sci Rep* 2017; **7**: 6085.

10 Kajiyama H, Utsumi F, Nakamura K, *et al*. Future perspective of strategic non-thermal plasma therapy for cancer treatment. *J Clin Biochem Nutr* 2017; **60**: 33–38.

11 Song K, Li G, Ma Y. A review on the selective apoptotic effect of nonthermal atmospheric-pressure plasma on cancer cells. *Plasma Med* 2014; **4**: 193–209.

12 Zucker SN, Zirnheld J, Bagati A, *et al*. Preferential induction of apoptotic cell death in melanoma cells as compared with normal keratinocytes using a non-thermal plasma torch. *Cancer Biol Ther* 2012; **13**: 1299–1306.

13 Li Y, Tang T, Lee H, Song K. Cold atmospheric pressure plasma-activated medium induces selective cell death in human hepatocellular carcinoma cells independently of singlet oxygen, hydrogen peroxide, nitric oxide and nitrite/nitrate. *Int J Mol Sci* 2021; **22**: 5548.

14 Rehman MU, Jawaid P, Uchiyama H, Kondo T. Comparison of free radicals formation induced by cold atmospheric plasma, ultrasound, and ionizing radiation. *Arch Biochem Biophys* 2016; **605**: 19–25.

15 Takamatsu T, Uehara K, Sasaki Y, *et al*. Investigation of reactive species using various gasplasmas. *RSC Adv* 2014; **4**: 39901–39905.

16 Tani A, Ono Y, Fukui S, Ikawa S, Kitano K. Free radicals induced in aqueous solution by non-contact atmospheric-pressure cold plasma. *Appl Phys Lett* 2012; **100**: 254103.

17 Anzai K, Aoki T, Koshimizu S, Takaya R, Tsuchida K, Takajo T. Formation of reactive oxygen species by irradiation of cold atmospheric pressure plasma jet to water depends on the irradiation distance. *J Clin Biochem Nutr* 2019; **64**: 187–193.

18 Terao J, Minami Y, Bando N. Singlet molecular oxygen-quenching activity of carotenoids: relevance to protection of the skin from photoaging. *J Clin Biochem Nutr* 2011; **48**: 57–62.

19 Jiménez-Banzo A, Sagristà ML, Mora M, Nonell S. Kinetics of singlet oxygen photosensitization in human skin fibroblasts. *Free Radic Biol Med* 2008; **44**: 926–934.

20 Arakane K, Ryu A, Hayashi C, *et al*. Singlet oxygen ($^1\Delta_g$) generation from coproporphyrin in *Propionibacterium acnes* on irradiation. *Biochem Biophys Res Commun* 1996; **223**: 578–582.

21 Younis MR, He G, Qu J, Lin J, Huang P, Xia XH. Inorganic nanomaterials with intrinsic singlet oxygen generation for photodynamic therapy. *Adv Sci (Weinh)* 2021; **8**: e2102587.

22 Li B, Lin L, Lin H, Wilson BC. Photosensitized singlet oxygen generation and detection: recent advances and future perspectives in cancer photodynamic therapy. *J Biophotonics* 2016; **9**: 1314–1325.

23 Flors C, Fryer MJ, Waring J, *et al*. Imaging the production of singlet oxygen *in vivo* using a new fluorescent sensor, Singlet Oxygen Sensor Green. *J Exp Bot* 2006; **57**: 1725–1734.

24 Niedre M, Patterson MS, Wilson BC. Direct near-infrared luminescence detection of singlet oxygen generated by photodynamic therapy in cells *in vitro* and tissues *in vivo*. *Photochem Photobiol* 2002; **75**: 382–391.

25 Ouchi A, Aizawa K, Iwasaki Y, *et al*. Kinetic study of the quenching reaction of singlet oxygen by carotenoids and food extracts in solution. Development of a singlet oxygen absorption capacity (SOAC) assay method. *J Agric Food Chem* 2010; **58**: 9967–9978.

26 Aizawa K, Iwasaki Y, Ouchi A, *et al*. Development of singlet oxygen absorption capacity (SOAC) assay method. 2. Measurements of the SOAC values for carotenoids and food extracts. *J Agric Food Chem* 2011; **59**: 3717–3729.

27 Lion Y, Delmelle M, van de Vorst A. New method of detecting singlet oxygen production. *Nature* 1976; **263**: 442–443.

28 Takajo T, Kurihara Y, Iwase K, Miyake D, Tsuchida K, Anzai K. Basic investigations of singlet oxygen detection systems with ESR for the measurement of singlet oxygen quenching activities. *Chem Pharm Bull (Tokyo)* 2020; **68**: 150–154.

29 Takajo T, Anzai K. Is there a simple and easy way to detect singlet oxygen? Comparison of methods for detecting singlet oxygen and application to measure scavenging activity of various compounds. *Arch Pharmacol Ther* 2020; **2**: 29–33.

30 Das KC, Das CK. Curcumin (diferuloylmethane), a singlet oxygen ($^1O_2$) quencher. *Biochem Biophys Res Commun* 2002; **295**: 62–66.

31 Joshi PC. Copper(II) as an efficient scavenger of singlet molecular oxygen. *Indian J Biochem Biophys* 1998; **35**: 208–215.

32 Gorbanev Y, O'Connell D, Chechik V. Non-thermal plasma in contact with water: the origin of species. *Chemistry* 2016; **22**: 3496–3505.

33 Uchiyama H, Zhao QL, Hassan MA, *et al*. EPR-spin trapping and flow cytometric studies of free radicals generated using cold atmospheric argon plasma and X-ray irradiation in aqueous solutions and intracellular milieu. *PLoS One* 2015; **10**: e0136956.

34 Kaneko T, Sasaki S, Takashima K, Kanzaki M. Gas-liquid interfacial plasmas producing reactive species for cell membrane permeabilization. *J Clin Biochem Nutr* 2017; **60**: 3–11.

35 Suenaga Y, Takamatsu T, Aizawa T, *et al*. Influence of controlling plasma gas species and temperature on reactive species and bactericidal effect of the plasma. *Appl Sci* 2021; **11**: 11674.

36 Hirano Y, Hayashi M, Tamura M, *et al*. Singlet oxygen generated by a new nonthermal atmospheric pressure air plasma device exerts a bactericidal effect on oral pathogens. *J Oral Sci* 2019; **61**: 521–525.

37 Saito K, Takeshita K, Ueda J, Ozawa T. Two reaction sites of a spin label, TEMPOL (4-hydroxy-2,2,6,6-tetramethylpiperidine-*N*-oxyl), with hydroxyl

doi: 10.3164/jcbn.22-111

radical. *J Pharm Sci* 2003; **92**: 275–280.
38 Ando T, Yoshikawa T, Tanigawa T, Kohno M, Yoshida N, Kondo M. Quantification of singlet oxygen from hematoporphyrin derivative by electron spin resonance. *Life Sci* 1997; **61**: 1953–1959.
39 Mukai K, Ishikawa E, Abe T, *et al*. Kinetic study of the quenching reaction of singlet oxygen by seven rice bran extracts in ethanol solution. Development of a singlet oxygen absorption capacity (SOAC) assay method. *Biosci Biotechnol Biochem* 2015; **79**: 2063–2072.
40 Karonen M, Mattila H, Huang P, Mamedov F, Styring S, Tyystjärvi E. A tandem mass spectrometric method for singlet oxygen measurement. *Photochem Photobiol* 2014; **90**: 965–971.
41 Nardi G, Manet I, Monti S, Miranda MA, Lhiaubet-Vallet V. Scope and limitations of the TEMPO/EPR method for singlet oxygen detection: the misleading role of electron transfer. *Free Radic Biol Med* 2014; **77**: 64–70.
42 Nakamura K, Ishiyama K, Ikai H, *et al*. Reevaluation of analytical methods for photogenerated singlet oxygen. *J Clin Biochem Nutr* 2011; **49**: 87–95.
43 Jablonowski H, Santos Sousa J, Weltmann KD, Wende K, Reuter S. Quantification of the ozone and singlet delta oxygen produced in gas and liquid phases by a non-thermal atmospheric plasma with relevance for medical treatment. *Sci Rep* 2018; **8**: 12195.